www.sciencemag.org/cgi/content/full/1124694/DC1

# Supporting Online Material for

## Spitzer Spectral Observations of the Deep Impact Ejecta

C. M. Lisse, J. VanCleve, A. C. Adams, M. F. A'Hearn, Y. R. Fernández, T. L. Farnham, L. Armus, C. J. Grillmair, J. Ingalls, M. J. S. Belton, O. Groussin, L. A. McFadden, K. J. Meech, P. H. Schultz, B. C. Clark, L. M. Feaga, J. M. Sunshine

Published 13 July 2006 on *Science* Express
DOI: 10.1126/science.1124694

**This PDF file includes:**

# Supplementary On-Line Material for "Spitzer Spectral Observations of the Deep Impact Ejecta"

**Spectral Modeling. (**The observed Spitzer spectrum is composed of emission features due to gas and dust in the comet's extended atmosphere, or coma, illuminated by the Sun. The majority of the observed spectrum is due to solid state emission resonances from the coma dust; we discuss this first. Two gaseous species, water and PAHs, were also detected. We discuss the contribution due to gas emission lines in a separate section below.)

The emission flux from a collection of cometary dust is given by

$$F_{\lambda,\mathrm{mod}} = \frac{1}{\Delta^2}\sum_i \int_0^\infty B_\lambda(T_i(a,r_*))Q_{abs,i}(a,\lambda)\pi a^2 \frac{dn_i(r_*)}{da}da$$

where $T$ the particle temperature for a particle of radius $a$ at distance $r_*$ from the central Sun, $\Delta$ is the range from Spitzer to the comet, $B_\lambda$ the blackbody radiance at wavelength $\lambda$, $Q_{abs}$ the emission efficiency of the particle due to its composition, $dn/da$ the differential particle size distribution (PSD) of the emitted dust, and the sum is over all species of material in the dust (1). The first problem encountered in treating the observations is isolating the signal due to Deep Impact. The material observed in the experiment consisted of the "ambient", or naturally emitted coma, plus the "ejecta", or material excavated from the interior of the comet at the impact site on the Tempel 1 nucleus. The ejecta spectrum was isolated by the simple method of subtracting the pre-impact spectrum from the post-impact spectrum. This method was found to be reasonable, as long term monitoring of the ejecta, or difference, spectrum showed a decay to zero over the first 100 hours after the impact. It is important to note that this method does not "remove the continuum" from the ejecta spectrum, but only separates the ejecta spectrum from the normal coma spectrum. It is also important to note that the problem of analysis of the spectrum was greatly simplified by the fact that all species were seen only in emission - the dust was self luminous in the thermal IR.

We are then left with a mid-IR ejecta spectrum that has structure due to the effects of dust particle temperature, composition, size, and porosity. Particle temperature influences the spectra by

emphasizing emission towards the peak of the blackbody function, and deemphasizing emission on the short wavelength side of the peak (i.e., "tilting" the spectrum towards long-wavelength end). In order to remove the gross effects of particle temperature on the data and instrument artifacts, we divided it by the featureless pre-impact continuum, scaled from the best-fit local LTE temperature of 235 K to the best-fit ejecta continuum temperature of 390K at I+45 min. (Note that in the detailed modeling, we treat each mineral species in precisely the same way, dividing the calculated flux contribution by a 390 K blackbody, so as to accurately compare the mineral species to the data. See the Particle Temperature effects section below.) Particle composition produces strong emission features at the wavelengths of the species crystal resonances, and affects what sizes of particles become optically thick, or essentially black, uniform emitters. Strong characteristic features found in the spectra, due to C=O, Si-O, H-O, etc. bond vibrations, were important in leading us to the appropriate species to test. Particle size and porosity determine the strength of the emission lines from a species versus the continuum, and provided the final "spectral shaping" constraint on the model. ***All three effects are important*** in obtaining a good model fit to the data, and are coupled by the $Q_{abs}$ and T(a) terms in SOM Eqn 1. The strength of the Spitzer data is that there are multiple crystal emission features and continua detected across the 5 - 35 μm wavelength range that must be fit simultaneously.

The emissivity spectrum of a linear mix of different species (allowing for the particle size, temperature, and porosity effects described in detail below), compared to our spectrum, was the ultimate test of each model run. The modeling problem was focused by our use of low resolution (R = 80 - 100) thermal IR spectroscopy; the features observed were too broad, except for contributions due to polyaromatic hydrocarbon molecules (PAHs), to be due to anything but solid state materials; and the features had to be in emission, because the ejecta was self-luminous and optically thin by I+45 minutes. The $\chi^2_\nu$ for 325 degrees of freedom (d.o.f.) at the 95% confidence limit (C.L.), i.e. the $\chi^2_\nu$ value for an acceptable model, was 1.13. For this work, we have chosen to work in "emissivity space" where the gross effects of particle temperature are removed by dividing the spectra by the best fit greybody to the continuum. This allows us to concentrate on the spectral features in the data indicative of the chemical composition, but can introduce complications if not treated carefully (see discussion on temperature effects below).

**Composition Effects.** Over 80 different species were tested for their presence in the ejecta. Consultations with members of the STARDUST team, and examination of the interplanetary dust

particle (IDP) literature (c.f. the review by Bradley 2002 (2)) and the astromineralogical literature (c.f. the review by Molster and Waters (3)) pointed to the most likely mineralogical candidates to be found in the ejected dust. Materials with emissions matching the strong features in the Spitzer emissivity spectra were also tested. The list of materials tested against the SST spectra included multiple silicates in the olivine and pyroxene class (forsterite, fayalite, clino- and orth-enstatite, augite, anorthite, bronzite, diopside, and ferrosilite); phyllosilicates (such as saponite, serpentine, smectite, montmorillonite, and chlorite); sulfates (such as gypsum, ferrosulfate, and magnesium sulfate); oxides (including various aluminas, spinels, hibonite, magnetite, and hematite); Mg/Fe sulfides (including pyrrohtite, troilite, pyrite, and niningerite); carbonate minerals (including calcite, aragonite, dolomite, magnesite, and siderite); water ice, clean and with carbon dioxide, carbon monoxide, methane, and ammonia clathrates; carbon dioxide ice; graphitic and amorphous carbon; and the PAH models of Li and Draine (4). Of these materials, a small, unique subset was found necessary to properly fit the Spitzer data. Sources for the data included the Jena (http://www.astro.uni-jena.de/Laboratory/OCDB), MGS/TES (http://tes.asu.edu), and Glaccum (private communication) spectral data libraries, as well as emission spectra supplied by Koike *et al.* and Chihara *et al.* for silicates (5); Kemper *et al.* for carbonates (6); Keller *et al.*, Kimura *et al.*, and Nuth *et al.* for sulfides (7); Li and Draine for PAHs (4); and Hanner (8) and Edoh (9) for amorphous carbon.

Whenever possible (~2/3 of the species tested), measured laboratory absorption and emission spectra of 1 μm powders was used for the comparison. Size effects were modeled using the radius and wavelength dependence of the relation

$$Emission(a,\lambda) = 1 - e^{-[2\pi a/\lambda][24nk/(\{n^2-k^2+2\}^2+4n^2k^2)]}$$

where n and k are the real and imaginary part of the index of refraction of the material at wavelength λ. In the small number of materials where direct spectra were unavailable, optical constants for the species were used instead, and the absorption spectra calculated using the full relation (10). Future work will include models using direct measurements of these species made in the laboratory.

Ca/Mg/Fe rich end members of each class of materials were used for the various models, with the amounts of each freely allowed to vary. For a non-endmember species present in the spectrum, this is equivalent to the assumption that the band positions between the species varies linearly with the

amount of Ca/Mg/Fe. On the other hand, Nuth *et al.* (11) have suggested one should expect **only** end members present in the crystalline form if vapor phase condensation plays an important role - and our method of analysis covers this possibility as well. But it should be made clear to the reader that by using a linear assumption, we are limited in that we cannot distinguish, for example, between an olivine sample composed of equal parts $Mg_2Si_2O_4$ and $Fe_2Si_2O_4$ and one composed of $MgFeSi_2O_4$. We do not claim to have found the **exact** mineral species with our technique; rather, we claim to have found the important mineral classes present in the ejecta, and the gross atomic abundance ratios.

Ground-based spectra of the 8-13 μm region during the DI encounter were successfully fit by Harker *et al.* (12) with a 3-component model consisting of amorphous olivine, amorphous pyroxene, and Mg-rich crystalline olivine (forsterite). This model had also been used previously to explain the mid-IR silicate emission from comet C/1995 O1 (Hale-Bopp) (13). We attempted to use this same model for our spectrum, but the best fit yielded an unacceptable $\chi^2_\nu$=4.3. The difference between their results and ours is due to SST's greater spectral range and better sensitivity: additional silicates are required in our model to fit the larger number of emission features detected at high fidelity. These extra features improve our derivation of the Fe:Mg ratio, the degree of crystallinity, and the existence of phyllosilicates, carbonates and sulfides, all of which are important clues to the state of the dust when it was incorporated into the comet (14). A similar attempt was made to use the olivine/pyroxene/PAH/FeO model of Malfait *et al.* (15), but again resulted in an unacceptable best-fit model with $\chi^2_\nu$=3.5.

**Particle Size Effects.** The size of the ejected dust was not uniform, and had to be modeled using an adjustable size distribution, *dn/da,* defined as the number of observed ejecta particles between size *a* and size *a+da*. (As the actual property measured in the Spitzer spectra is the product of the particle *surface area * dn/da*, this is the function that was used and adjusted in the models.) In practice, this meant that independent values of *dn/da were adopted at each value* (0.1, 0.2, 0.5, 1, 2, 5, 10, 20, 50, 100, 200, 500, 1000) μm, a new model calculated, and the result compared to the observed emissivity distribution. The emission from one PSD is calculated as providing all the observed flux. (There is no assumption of two separate PSDs, one for the sharp features and one for the continuum, with so distinct chemical compositions, as is sometimes assumed. It is difficult to determine the chemical composition of optically thick material, as the characteristic emission lines lose contrast with the continuum. I.e., the emission from any material which is suitably optically thick approaches

blackbody behavior, as the large size limit the crystal vibrational modes "fill-in" the density of states between the modes found in the single unit cell case.)

The effects of different-sized particles was clearly seen in the data; small particles create sharp spectral features, but contribute little to the continuum, while large particles act in the opposite fashion. Model fits without large particles do not fit the long wavelength continuum from 20 - 35 μm well; model fits without small particles do not reproduce the strong spectral features. It is immediately clear from the presence of the strong spectral features, as opposed to the smooth, featureless pre-impact coma spectrum, that the ejecta is enhanced in small particles.

The best-fit size distribution has a significant number of 0.1 - 1.0 μm particles and a maximum in emitted particle surface area in the 1-5 μm particle range (SOM Figure 1), consistent with the size estimated by radiation pressure effects on the ejecta cloud determined by Richardson *et al.* (16), the dynamical particle size seen by ground-based observers (17), and the effective ice particle size found by Sunshine *et al.* in the DI HRI-IR spectrometer data (18). The best-fit points follow a power law slope at the large particle end with $dn/da \sim a^{-4.5\pm0.2}$. This best-fit power law is much steeper than that of the pre-impact coma ($dn/da \sim a^{-3.0\pm0.45}$ (19) and even steeper than that found for dust emission from C/1995 O1 (Hale-Bopp) or for the in situ measurements of the 1P/Halley size distribution in the 1- 20 μm range, although both peak at about 1 μm (20). The ejecta emitting surface area is dominated by the excess 0.5 - 10 μm particles, as is the total mass. The presence of the extremely sharp spectral features is a direct consequence of the increase in the small particles - large particles are optically thick to mid-IR radiation, and demonstrate only featureless, blackbody-like emission behavior (1). The sharp proportional increase in the number of small particles in the ejected dust is good evidence for de-aggregation of larger particles into the smaller component sub-particles, a process which would remove large particles from the ejecta and add small ones.

A check of the particle size distribution was made by summing the total mass seen in the PSD, and comparing the result to the amount of dust and gas mass estimated to have been ejected by other groups. From the normalization of the model spectrum to the observed flux, we derive the total mass of the observed dust grains and the minimum Dust/Gas ratio in the Spitzer 10" x 10" spectrometer beam as a function of the adopted maximum particle size (SOM Table 1). We find that the minimum range of particles that must be included to obtain a good spectral fit is $0.1 < a < 10.0$ μm (maximum

ejected particle mass 10 ng), which gives a minimum total ejected mass of 8 x $10^5$ kg.

By comparison, Sugita *et al.* (21), using 8 - 20 μm photometric measurements in 4 passbands, found a best-fit power law PSD similar to our result, with slope *dS/dloga* = -1.5 to -1.6, but used a small particle cutoff at 1 μm. Their total released dust mass ranges from ~5 x$10^5$ to 7 x $10^7$ kg, for a largest emitted particle size of 10 μm and 1m, respectively. Harker *et al.* (12) , using 8 - 13 μm ground based spectroscopy from the Gemini North telescope with poorer sensitivity than the Spitzer measurements, estimated a released dust mass of 1 x $10^4$ - 1 x $10^6$ kg, consistent with our findings (SOM Table 1). Keller *et al.* (private communication) have argued for a minimum β value of $10^{-3}$ in their ROSETTA imaging of the ejecta, implying a maximum particle size on the order of 500 μm, a maximum ejected particle mass of 1 mg, at least 7 x $10^6$ kg of dust emitted, and a minimum D/G in the ejecta of 1.4 for a total mass of ejected gas equal to 5 x $10^6$ kg, but this remains as unpublished work. The $\chi^2_\nu$ value for a spectral model using 1 mg as the largest particle is 2% larger than the best fit result obtained with a 10 μm upper limit, An ejected particle mass on the order of a milligram is certainly reasonable, given that the DI impactor hit at least four particles weighing a mg or more on its way in.

**Particle Temperature Effects.** If a dust particle is small or lacks emission bands in the thermal IR, then its color temperature rises above that of a blackbody in LTE because these factors restrict the ability of the particle to re-emit absorbed sunlight (1,22). As particles grow larger, their color temperature decreases towards LTE as their emission bands become optically thick, and they approach blackbody behavior. Contrarily, sublimation of volatile ices removes energy from the particles, producing a net reduction in the color temperature (22). Wooden *et al.* (13) and Harker et al (12) found similar concerns with spectral models of the dust emitted by C/1995 O1 (Hale-Bopp) and Harker *et al.* also employed this approach in fitting the Gemini observations of the DI-Tempel 1 encounter (12).

For modeling the SST spectra, we allowed the temperature of the smallest 0.1 μm particles in the model to vary freely. It was found to be elevated for all species compared to LTE. This is due to the emissivity drop-off at IR wavelengths, restricting the ability of the smallest particles to dump the energy absorbed from sunlight at optical wavelengths as re-emitted heat radiation. At the other size extreme, the 1000 μm size of the largest particles was chosen to ensure that the dust was optically

thick, and thus at the LTE temperature (or sub-LTE, in the case of water ice, due to sublimation). The temperature of the intermediate particles was then interpolated between these two extremes using energy balance of the incoming sunlight and the re-radiated thermal emission.

The emissivity model determined by the composition, particle size distribution, and temperature was then compared to the SST spectrum, after division by a 390K blackbody to match the treatment of the SST data. Best-fit temperatures with accuracies of +/- 5K were found by optimizing the model fit to the emissivity data. We found that the smallest particles of amorphous carbon dust in the beam are very hot, about 420K; most silicates, the carbonates, and the sulfides are warm, at 340 K, similar to the continuum temperature found in the NASA/IRTF spectra taken on the night of impact (23); the pyroxene ferrosilite is cooler, 290 K, similar to the findings of Wooden *et al.* for comet Hale-Bopp's dust (13,14); LTE is about 235K; and the ejected water ice, cooled by sublimation, is the coldest at 220 K, similar to the Deep Impact temperature estimates of Sunshine *et al.* (18).

**Porosity Effects.** The effects of porosity on the emission of IR radiation from dust particles is subtle, Vacuum filled pore spaces in dust particles act to "mix in" the dielectric constant of free space with that of the surrounding dust solids. The net effect is to reduce the strength of the characteristic emission modes of the solid material. This effect is wavelength dependent, as the wavelength of the emitted IR radiation at 35 μm is large enough to average over the whole micro-structure of the dust particles seen in the T1 ejecta, while radiation at 5 μm will sense some of the particles as single units, and others as not.. For the modeling, our work was greatly simplified by the finding that the only porosity value that came close to fitting the observed ejecta spectrum was 0 - implying that we were observing mostly tiny, solid dust particles, with size 0.1 - 5.0 μm. This is consistent with the scenario of the large, loose, porous aggregate dust particles having been disrupted by the ejecta event into their individual solid subunits. A preponderance of small, solid dust particles was also found for the copious dust emitted from comet C/1995 O1 (Hale-Bopp) (24).

**Gas emission lines.** In general, single emission lines suffer from spectral dilution in the low resolution, large wavelength grasp Spitzer spectra. It is much more likely for broad emission features due to crystalline resonances to be detected. However, there are a few special cases - like the very broad water gas feature at 6 μm (similar to the broad 3 μm emission/absorption feature of water but less well known), and a dense P/Q/R branch system, like for PAHs - that may be detectable. The

strength of a molecular feature will also depend strongly on the abundance of the species in the coma gas. Thus we have tested the Spitzer spectrum, using the JPL HITRAN line lists, for the presence of emission from the strongest features of the most abundant gaseous species in the coma - water gas, carbon dioxide gas (carbon monoxide gas does not have strong emissions in the 5 - 35 μm range), and PAHs. Once a line is detected, the number of gas molecules in the beam is calculated using the relation

$$PhotonNumberFlux = \frac{F(Jy) * d\lambda}{h\lambda} = \frac{gN_{mol}}{4\pi\Delta^2 r_h^2}$$

where F is the flux in the line, dλ is the width of the line, λ is the center wavelength of the band, g is the g-factor for the band, $N_{mol}$ is the number of molecules in the beam, Δ is the Spitzer - comet distance, and $r_h$ is the comet-Sun distance.

For Tempel 1, we found evidence, at the 5-sigma level, of water gas emission from the $\nu_2$ emission band at 6 μm. Removing the water gas changes the $\chi^2_\nu$ value for the model from 1.05 to 1.22, so the detection, while significant at the 95% C.L. is not terribly strong. On the other hand, since water gas is clearly in the coma as the major molecular species liberated by the impact, and is emitting radiation, it is comforting that we find evidence for it in our modeling. The detection of 6 x $10^5$ kg of water in the 10" x 10" Spitzer beam at I + 45 minutes is consistent with the work of other groups, notably the ROSETTA measurements reported by Keller *et al.* and Kuppers *et al.* (25), and the Deep Impact results by Sunshine *et al.* (18).

We can rule out the 6 μm peak as originating from water ice, as the emission at wavelengths shorter than the broad 10 -16 μm feature from water ice is damped by the low temperature of the solid ice, ~220 K, and a significant contribution at 6 μm would mean a huge contributed flux at 10-16 μm which is not seen. We can similarly rule out emission features due to water ice : $CO_2$, CO, or $CH_4$ clathrates at nearby wavelengths.

The weakness of the water gas detection for what is a relatively strong gas emission feature from the majority coma gas species does suggest that it is probably very difficult to detect any other species using the low-resolution IRS data. E.g., we did not find any convincing evidence for carbon dioxide emission lines, including the strong fundamental at 14.97 μm (g-factor about ½ the magnitude as for

the $H_2O$ $\nu_2$ band), as $CO_2$ is typically only a few % abundant vs. water in cometary comae. Early in our studies, we searched, without success, for emission from the gaseous species CS, which has a very strong resonance at 6.5 μm one to two orders of magnitude stronger than the $H_2O$ $\nu_2$ band, but a very low abundance (~0.1% of water). Our analysis did find emission from PAHs at an equivalent PPM level, but this was aided by the very strong resonances with a dense number of emission lines centered at multiple wavelengths near 6.2, 7.7, 8.6, and 11.3, and 12.4 μm.

**Final composition results.** The final results of our modeling can be seen in Figure 3 (model vs. total ejecta emissivity at I+45 minutes) and Figure 4 (non-silicate model vs the silicate removed ejecta spectrum). Both figures are to the same scale, and the need for the residual figure can be seen in the subtlety of some of the smaller features, like the PAH and water gas emissions, versus the extremely strong silicate emission features, which account for more than 60% of the total observed energy. In the residuals, a good match is found at 5 - 15 μm between the predicted PAH and carbonate features and the data. The long wavelength residuals are consistent with the expected broad ningerite feature, but sharper features at 22.5, 24, 26.5, 28, 29, 30.5, 31.5, and 33 μm need to be accounted for. The combination of water ice and amorphous carbon emission produces the bulk smooth of the inter-feature continuum at 5- 15 μm, while sulfides, carbonates, and at the longest wavelengths, water ice form the long-wavelength continuum. The temperature of all components except for the water ice, amorphous carbon, and ferrosilite were found to be ~340 K, somewhat elevated above LTE, but close enough to each other to suggest a common heating history or thermal link between them.

*From species comprising the best-fit model, we have found the following as the majority species in the Tempel 1 ejecta:* crystalline silicates like forsterite, fayalite, orth-enstatite, diopside, ferrosilite and amorphous silicates with olivine and pyroxene like composition; phyllosilicates similar to nonerite; sulfides like ningerite; carbonates like magnesite and siderite; water gas and ice; amorphous carbon (and potentially native Fe:Ni; and ionized PAHs.

*And have not found any statistically convincing evidence for the following species :* silicates (such as clino-enstatite, augite, anorthite, bronzite); phyllosilicates (like saponite, serpentine, smectite, montmorillonite, and chlorite); sulfates (like gypsum, ferrosulfate, and magnesium sulfate); oxides (including various aluminas, spinels, hibonite, magnetite, and hematite); sulfides (including

stoichiometric troilite and pyrite); carbonate minerals (including calcite, aragonite, dolomite); water ice with $CO_2$, CO, $CH_4$, and $NH_3$ clathrates; $CO_2$ gas and ice; CS gas; graphitic carbon; and neutral PAHs.

## References and Notes :


1. Lisse, C.M. *et al.*, *Ap J* **496**, 971 (1998)

2. Bradley, J.P., In *Astromineralogy*, *Lecture Notes in Physics* **609**, ed. T.K. Henning.,pp. 217 -235 (2002)

3. Molster, F.J. and Waters, L.B., In *Astromineralogy Lecture Notes in Physics* **609**, ed. T.K. Henning., pp. 121 - 170 (2002)

4. Li, A. and Draine, B.T., *ApJ* (2007, submitted)

5. Koike, C., Astronomy and Astropysics, **363**, 1115 (2000); Koike, C. *et al.* , *Astron. Astrophys* **399**, 1101 (2002); Chihara, H., *et al.*, *Astron. Astrophys* **391**, 267 (2002)

6. Kemper, F., *et al.*, *Nature* **415**, 295 (2002)

7. Nuth, J.A. *et al.*, *ApJ Lett.* **290**, L41 (1985); Keller, L.P. *et al.* 2002. *Nature* **417**, 148-150 ; Kimura, Y. *et al.*, *Astron. Astrophys.* **442**, 507 (2005)

8 Hanner, M. S., *et al.*, *Adv. Space Res. 4*, No. **9**, 189 (1984)

9 We have used the optical constants of Edoh T., PhD Thesis, University of Arizona (1983), for this work.

10. Koike, C. *et al.*, *Icarus* **114**, 203 - 214 (1995); Koike, C. *et al. Mon. Not. R. Astr. Soc.* **239**, 127 - 137 (1989)

11. Nuth, J.A. *et al.*, 2002. *Meteoritics and Planetary Science* **37**, 1579 - 1590

12. Harker, D.E., *et al.*, *Science* **310**, 278 (2005)

13. Wooden, D. *et al.*, *ApJ* **517**, 1034 (1999); Harker, D.E., *et al.*, *ApJ* **580**, 579 (2002)

14. Hanner, M.S., *et al.*, *ApJ* **502**, 871 (1998); Wooden, D., *et al.*, *Icarus* **143**, 126 (2000)

15. Malfait, K. *et al.* 1998. *Astron. Astrophys.* **332**, L25 (1998)

16. Richardson, J. *et al.*, *"Modeling the Ballistic Behavior of the Solid Ejecta from the Deep Impact Cratering Event", Icarus* (2006, in preparation)

17. Meech, K.J., *et al.*, *Science* **310**, 265 (2005)

18. Sunshine, J.S., *et al.*, *Science* **311**, 1453 (2006)

19. Lisse, C.M., *et al.*, *Space Science Reviews* **117**, 161 (2005b)

20. Lisse, C.M., *et al.*, *Earth, Moon, and Planets* **78:1-3**, 251 (1999); Harker, D.E., *et al.*, *ApJ* **580**, 579 (2002); McDonnell *et al.* in *Comets in the Post-Halley Era*, 1043 (1991).

21. Sugita, S., *et al.*, *Science* **310**, 274 (2005)

22. Lien, D.J., *ApJ* **355**, 680 (1990)

23. Fernandez, Y.R., *et al.*, Icarus (2007, submitted)

24. Williams, D.M. *et al.*, *Ap J Lett* **489**, L91 (1997); Lisse, C.M., *et al.*, *Earth, Moon, and Planets* **78:1-3**, 251 (1999)

25. Keller, H.U. *et al.*, Science 310, 281 (2005); Kuppers, M. *et al.*, Nature 437, 987 (2005)

**SOM Table 1 - Mass and D/G as a Function of Largest Particle Emitted**

| $a_{max}$ (um) | $\beta_{min}$ † | $Mass_{max}$ (g) | $M_{total}$ (kg) | D/G* |
|---|---|---|---|---|
| 0.50 | 0.94 | 1.3e-12 | 6.8e4 | 0.12 |
| 1.00 | 0.47 | 1.0e-11 | 2.2e5 | 0.38 |
| 2.00 | 0.24 | 8.4e-11 | 4.5e5 | 0.77 |
| 5.00 | 0.094 | 1.3e-09 | 6.7e5 | 1.15 |
| 10.00 | 0.047 | 1.0e-08 | 7.8e5 | 1.32 |
| 20.00 | 0.024 | 8.4e-08 | 8.4e5 | 1.45 |
| 50.00 | 0.0094 | 1.3e-06 | 9.1e5 | 1.57 |
| 100.00 | 0.0047 | 1.0e-05 | 9.4e5 | 1.62 |
| 200.00 | 0.0024 | 8.4e-05 | 9.6e5 | 1.66 |
| 500.00 | 0.00094 | 1.3e-03 | 9.8e5 | 1.70 |
| 1000.00 | 0.00047 | 1.0e-02 | 9.9e5 | 1.71 |

† - Assumes $\beta = 0.47/a(um)$

* - Determined using g-factor of $2.2 \times 10^{-4}$, normalization of $5.8 \times 10^{5}$ kg total water gas, $7.8 \times 10^{5}$ kg total dust mass in beam.

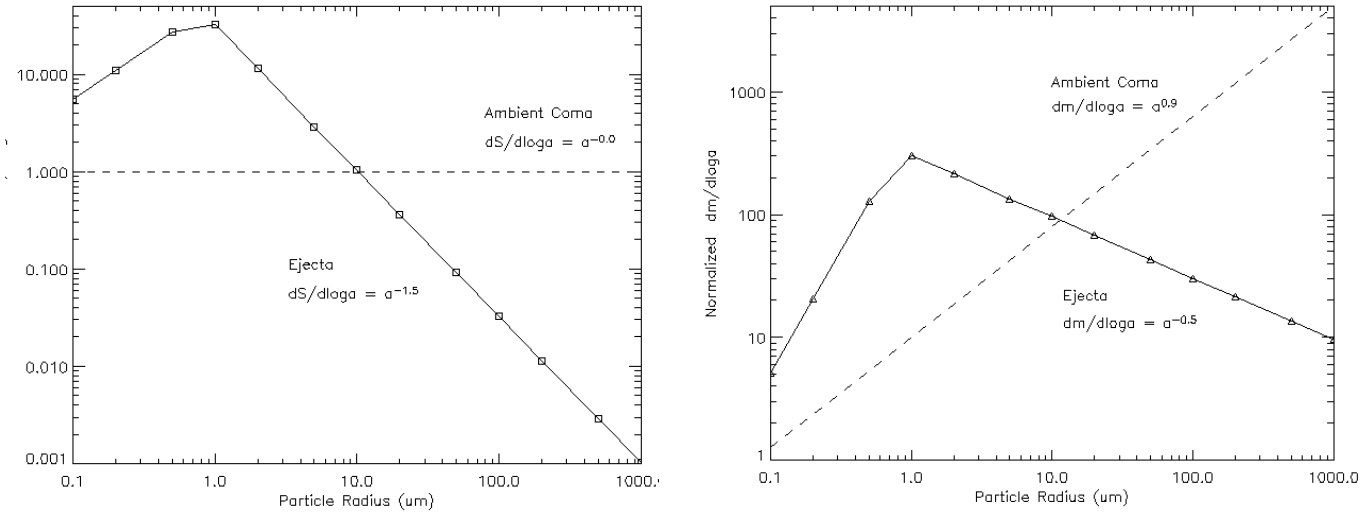


**Figure 1 SOM - Best Fit Dust PSDs** for the natural, ambient coma and DI-ejected dust. Left - Surface area size distribution, the quantity directly measured in the Spitzer observations. Right - inferred mass distribution. Sold line - ambient coma (i.e. pre-impact dust emission). Symbols - ejected dust due to the impact. The absolute number size distribution predicts 1 particle of radius 7 cm in the beam; the ejected material was all very small, with about $10^{22}$ 0.1 um particles ejected.